100 Gbit/s PAM-4 Linear Burst-Mode Transimpedance Amplifier for Upstream Flexible Passive Optical Networks

Gertjan Coudyzer, Michiel Verplaetse*, Borre Van Lombergen, Robert Borkowski, Thibaut Gurne, Michael Straub, Yannick Lefevre, Peter Ossieur, René Bonk, Werner Coomans, Jochen Maes, Xin Yin

***Abstract*—Next-generation passive optical networks (PONs) with upstream rates of 50 Gbit/s and beyond will require a new class of burst-mode transimpedance amplifiers (BMTIAs) that are linear to enable (digital) equalization of channel impairments. Such linear BMTIAs also enable higher-order modulation formats like 4-level pulse amplitude modulation (PAM-4). In this paper, we demonstrate operation of a novel linear BMTIA integrated together with a commercial off-the-shelf 25G-class avalanche photodiode (APD), achieving 50 Gbit/s non-return-to-zero (NRZ) operation with a sensitivity of -23.7 dBm optical modulation amplitude (OMA) and dynamic range exceeding 21.7 dB and 100 Gbit/s PAM-4 operation with a sensitivity of -15.8 dBm OMA and dynamic range exceeding 15.4 dB, both at a bit error ratio (BER) of 10^{-2}. In addition, fast burst-mode gain-control and balancing circuits limit loud-soft sensitivity penalties in the case of AC-coupled circuits to less than 1.3 dB. The chip was designed in a 0.13 µm SiGe:C BiCMOS technology, has an area of 1.2×1.7 mm² and consumes between 260 mW and 310 mW. This receiver paves the way to a next-generation class of BMTIAs, supporting the ITU-T G.9804.3 Amd 1 standard.**

***Index Terms*—burst-mode, transimpedance amplifiers, 4-level pulse amplitude modulation, passive optical networks, access networks**

I. Introduction

In recent years, PON have been increasingly used to deliver high-speed internet access in a cost-efficient manner through fiber-to-the-home (FTTH). Fiber sharing is key to achieving a mass roll-out in access networks. As bandwidth demand increases, so will the demand for these upstream data rates, in particular for services to support critical network infrastructure, next generation fronthaul, industrial factories and others [1], [2].

Upstream transmission in PONs uses time-division-multiple-access (TDMA), where the received signal at the optical line terminal (OLT) receiver consists of a stream of consecutive bursts from different optical network units (ONUs). The challenges related to this burst-based transmission complicate the increase of upstream transmission speeds in comparison to continuous mode operation. Individual bursts are characterized by a very wide dynamic range of the optical power due to the differential path loss of the optical distribution network (ODN) and variations of the ONU transmitter launch powers. Bursts which are received at the OLT can quickly succeed each other within tens of nanoseconds, while exhibiting optical power variations of around 20 dB [3].

In these networks, the analog front-end containing the burst-mode receiver becomes an enabling factor in progressing towards higher-tier upstream transmission rates. Recently, 50G US has been consented in Amd 1 of ITU-T G.9804.3, which defines a 50G NRZ variant. To compensate for distortions due to the limited bandwidth of the opto-electronics such as the avalanche photodiode (APD), fiber chromatic dispersion and its interaction with modulator chirp [4], [5], [6], equalization will be required. This demands for a class of linear burst-mode receivers, which enables not only equalization but allows for multi-level modulation schemes such as PAM-4, increasing link capacity for all users [7], or for selected users in an opportunistically flexible PON. Such a flexible receiver [8] can adapt its line rate up to 100 Gbit/s depending on the channel loss by choosing different modulation and forward-error-correction (FEC) variants. Therefore, this generation of linear receivers allows such flexibility by supporting both NRZ and PAM-4 as modulation formats.

As present-generation burst-mode receivers used in e.g. XGS-PON and 25GS-PON are not required to be linear due to the NRZ modulation and the lack of need for equalization, non-linear transimpedance amplifier architectures using simple gain and input offset current control schemes can be used in combination with limiting post-amplifiers. Handling the fast transients arising due to the rapidly changing optical average power is a challenge for any burst-mode receiver design, even more so for a linear burst-mode receiver. Furthermore, it also needs to ensure that the output swing and offset voltage is precisely adjusted on a burst-per-burst basis such that the resulting signal is optimally conditioned for sampling by a slicer or an analog-to-digital converter (ADC). Care must be taken not to introduce non-linearities due to e.g. compression in the subsequent amplifier stages.

Burst-mode reception was previously shown either using an optical preamplifier without transimpedance amplifier (TIA)

G. Coudyzer, B. Lombergen, P. Ossieur and X. Yin are with imec - Ghent University, 9052 Ghent, Belgium (email: gertjan.coudyzer@imec.be).

M. Verplaetse, T. Gurne, Y. Lefevre, W. Coomans, J. Maes are with Nokia Bell Labs, Copernicuslaan 50, 2018 Antwerp, Belgium (email: michiel.verplaetse@nokia-bell-labs.com).

M. Straub, R. Bonk are with Nokia Bell Labs, Magirusstr. 8, 70469 Stuttgart, Germany.

R. Borkowski is with Nokia Bell Labs, 600 Mountain Ave, Murray Hill, NJ 07974, USA.

Supported by VLAIO projects SPIC and SPARTA (HBC.2020.2197 and HBC.2022.0428)

Manuscript received XXXX XX, XXXX; revised XXXX XX, XXXX.

* with equal contribution.

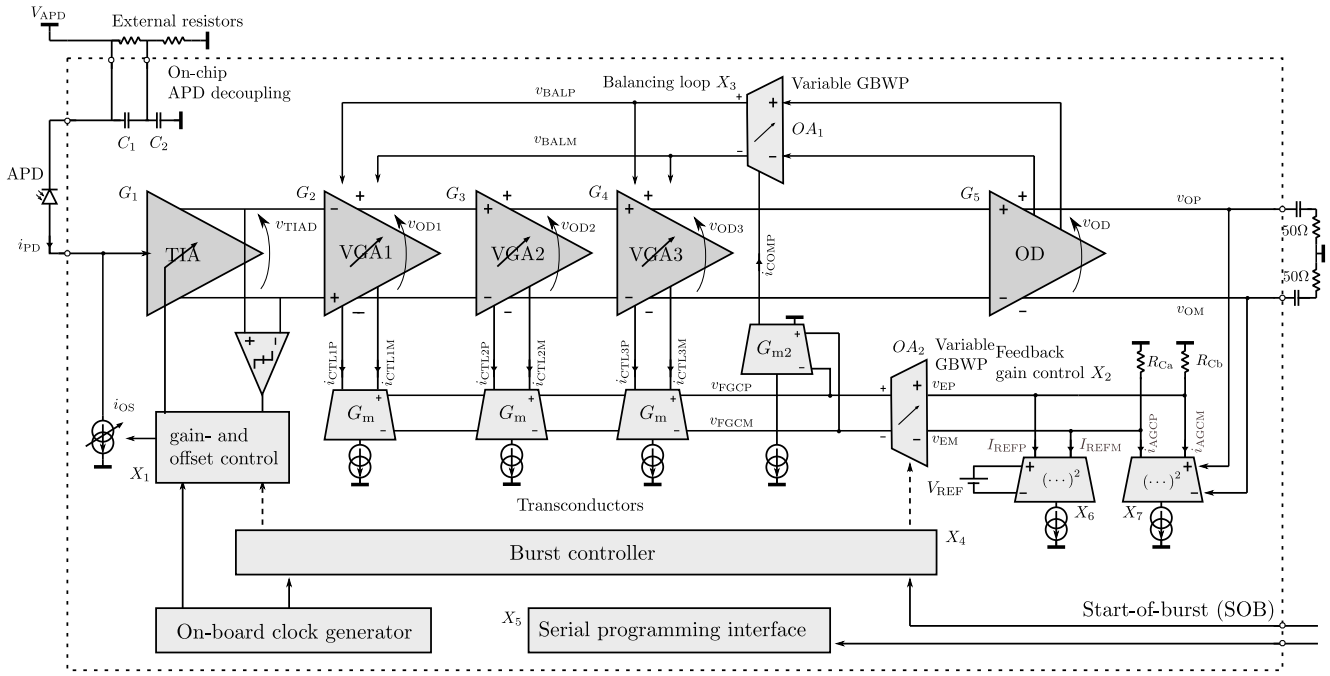

Fig. 1: Overall architecture of the BMTIA.

[9] for 50 Gbit/s; in the context of data centers with a limiting (nonlinear) TIA, lacking support for an extended PON dynamic range [10], [11]; limiting non-linear NRZ burst-mode receivers for PON up to 25 Gbit/s [12], [13], [14]; or using a PAM-4 linear BMTIAs up to 10 GBd [15] or 25 GBd [16], [17], [18].

In this paper, which is an extension to [19], using a novel linear BMTIA assembled together with an off-the-shelf 25G-class APD, we demonstrate burst-mode reception of 50 Gbit/s NRZ or 100 Gbit/s PAM-4. In addition to our previous paper, in Section II the receiver architecture of the BMTIA is discussed in more detail. Experimental setup and results are described in Section III and Section IV. Furthermore, we extended the experimental analysis to include a study of loud-soft consecutive bursts and the sensitivity penalty it leads to.

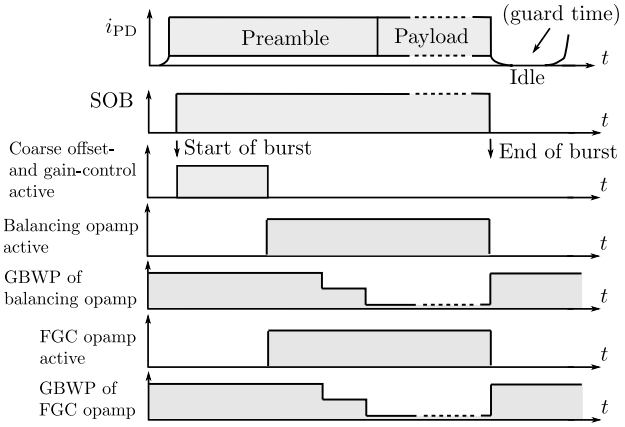

Fig. 2: Burst timing diagram.

II. Architecture

Fig. 1 shows the overall architecture of the implemented BMTIA. A first transimpedance amplifier stage G_1 converts the photocurrent i_{PD} into a differential output voltage v_{TIAD}. Its gain and input offset current is adjusted in a coarse offset- and gain control system X_1 to accommodate to the incoming burst strength. The resulting signal is then amplified in a series of three variable-gain-amplifiers (VGAs) G_2, G_3, G_4, whose gain is controlled through i_{CTLx} via a gain-control system X_2 which regulates the output signal power. An output driver G_5 provides $50\,\Omega$ matching for interfacing with external circuits. Any remaining differential offset voltage present at its output will be eliminated by means of a feedback balancing loop X_3. The BMTIA achieves a total transimpedance gain ranging from $39\,\mathrm{dB}\Omega$ to $80\,\mathrm{dB}\Omega$, to cope with a wide optical dynamic input range, exceeding $20\,\mathrm{dB}$. The different systems are activated by a central burst controller X_4, which receives an external start-of-burst (SOB) signal at the beginning of each received burst. Through a serial programming interface (SPI) interface X_5 the chip settings can be modified for optimal performance.

The burst-mode operation is illustrated in Fig. 2. An external SOB signal is provided by the OLT medium access control (MAC) controller, which indicates the presence of an optical burst at the input of the BMTIA. At this point, the coarse offset- and gain-control system X_1 initializes the front-end TIA to a low gain mode and determines whether the gain can be increased without compression of the signal. In a second step, a proper offset current i_{OS} is determined to obtain an approximately balanced differential signal at the output of the front-end TIA.

In order to optimally condition the signal for use by an ADC or slicer while maintaining linearity, the output swing must be accurately controlled to a desired constant value for all

bursts. For this purpose, a fine gain control (FGC) loop X_2 using opamp OA_2 is activated which controls the analog gain control currents for each of the VGAs. Using two identical Gilbert-cell-type power detectors X_6 and X_7, a feedback loop modifies the gains of the VGAs until the root mean square (RMS)-value of v_{OD} equals an internal reference voltage V_{REF}. To allow digital equalization at the receiver and PAM-4 modulation, we previously demonstrated the linearity requirements expressed in total harmonic distortion (THD) to mitigate the power penalty in presence of limited bandwidth of opto-electronic components and chromatic dispersion [4]. As the BMTIA has been developed for this purpose, it has been designed for linearity with a target THD of $< 5\%$ (fundamental tone of $5\,\mathrm{GHz}$) for bursts with an optical power up to $-9\,\mathrm{dBm}$ (assuming $8\,\mathrm{A/W}$ nominal photodiode responsivity). Alternatively, level separation mismatch ratio (RLM) can be used to specify linearity, which can be investigated in future work.

In addition to a well-controlled output swing, the signal must be well-balanced. With the balancing system X_3 and opamp OA_2, the differential output offset voltage is regulated to zero. As will be shown in Section IV-C, any residual output offset voltage will cause burst wander when AC-coupling the receiver to external circuitry, with settling times approaching the lower cut-off-frequency of the DC-blocks. In particular for loud-soft burst transitions, this may significantly increase the BER and cause sensitivity penalties.

Using the receiver in burst-mode implies that these control loops must settle within a reasonable amount of time, to minimize the required preamble time and overhead in each burst. To eliminate the trade-off between this settling time and baseline wander (for the balancing control) or gain modulation (for the FGC), the control opamps OA_1 and OA_2 operate under varying bias currents. In the balancing loop for instance, the bias current I_B modifies the gain-bandwidth product ($GBWP$) of OA_1 according to:

$$GBWP = \frac{g_m(I_B)}{2\pi C_L} K_{\mathrm{VGA}} \tag{1}$$

Where K_{VGA} is the datapath gain of the VGAs and $g_m(I_B)$ is the transconductance of the opamp input stage, which is a function proportional to I_B. Initially, the opamp operates at a high speed with a $GBWP$ of $220\,\mathrm{MHz}$ for the control loop. This mode enables the opamp to quickly react and correct the output offset voltage. After settling, the $GBWP$ of the opamp can be reduced to limit baseline wander during the payload.

An issue that must be taken care of is the fact that the balancing loop must operate at the same speeds, irrespective of the gain in the different VGAs. These gains will vary over the required dynamic input range, easily exceeding at least $8\,\mathrm{dB}$ per stage. To achieve this, a second injection point for the offset compensation is added after the third VGAs in case the VGAs gain is very low.

Based on the bahavior of the measured output waveforms of the BMTIA, a total settling time of $150\,\mathrm{ns}$ is estimated, mainly limited by the speed of the coarse offset- and gain-control (COGC) process.

The bandwidth of APD/BMTIA assemblies using a shunt-feedback topology is typically limited due to the interconnect between the BMTIA and APD. The anode and cathode bondwires together with the photodiode capacitance form a resonance in the frequency domain, beyond which a sharp roll-off can be observed. This resonance frequency can be given as:

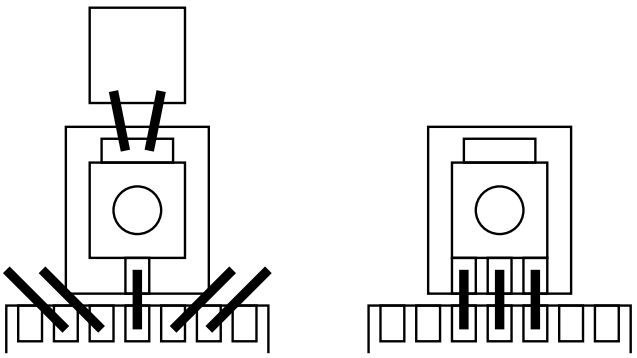

(a) Off-chip biasing. (b) On-chip biasing.

Fig. 3: On-chip biasing of the APD, leading to reduced bondwire inductance L_{bw}.

$$f_{\mathrm{p}} = \frac{1}{2\pi\sqrt{L_{\mathrm{bw}} C_{\mathrm{pd}}}} \tag{2}$$

In this equation, L_{bw} is the anode and cathode bondwire inductance and C_{pd} is the photodiode capacitance, both which are external to the BMTIA design. To allow 50 GBd operation and higher it is essential that these parameters are minimized. In PIN-photodiodes the bondwire inductance can be lowered by closely coupling the anode and cathode bondwires and providing the cathode bias on-chip, but the high voltages required for APD devices typically lead to them being biased off-chip (resulting in higher bondwire inductance, as shown in Fig. 3). In our design, the $> 20\,\mathrm{V}$ bias is decoupled on-chip using two on-chip metal-insulator-metal (MIM) capacitors C_1 and C_2 (in Fig. 1) in series to lower the voltages over the capacitors, thus avoiding dielectric breakdown. To ensure that the voltage is equally split between the two capacitors, external resistors are used instead of on-chip resistors, as these are not subject to well breakdown. Due to the high voltages present, the on-chip decoupling capacitors are isolated from the rest of the integrated circuit (IC).

The chip is wirebonded together with a commercial 25G APD on a printed circuit board (PCB) assembly shown in Fig. 4. The assembled APD (with performance metrics like capacitance and dark current in line with 25G-class commercial APDs) was biased at a fixed voltage to get the best responsivity within the breakdown limits of the device (measured responsivity of $9.3\,\mathrm{A/W}$). Using a supply voltage of $2.5\,\mathrm{V}$ for the datapath and $1.2\,\mathrm{V}$ for the digital cores, the BMTIA consumes between $260\,\mathrm{mW}$ and $310\,\mathrm{mW}$, depending on the optical power of the incoming bursts.

III. Measurements

The linear BMTIA is evaluated in an experimental setup shown in Fig. 5. An electrical 50 GBd NRZ or PAM-4 signal

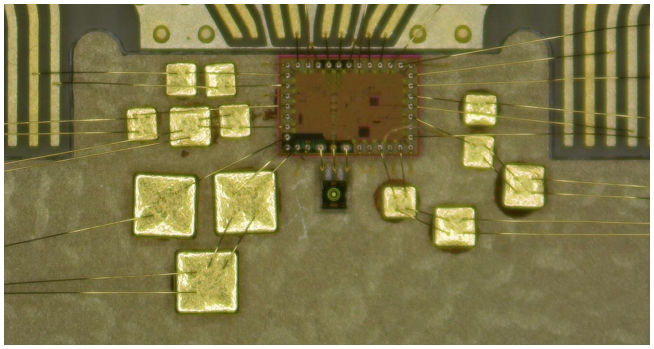

Fig. 4: BMTIA together with APD in a wirebonded assembly. Die dimensions: $1.2\,\mathrm{mm} \times 1.7\,\mathrm{mm}$.

with a period of 2^{15} symbols is generated. A pre-emphasized digital-to-analog converter (DAC) is used and drives a Mach-Zehnder-modulator (MZM) with a bandwidth of $35\,\mathrm{GHz}$, which is supplied with an O-band distributed feedback (DFB) laser source at $1308.7\,\mathrm{nm}$. The pre-emphasis filter is optimized independently for NRZ and PAM-4, which results in different outer extinction ratios for both modulations. For NRZ, the transmitter eye closure (TEC) evaluated in an optical back-to-back case as per ITU-T G.9804.3 (50G DS) is measured to be $2.4\,\mathrm{dB}$, and the extinction ratio (ER), evaluated on the longest sequence of consecutive identical digits of the signal, was measured to be $10.6\,\mathrm{dB}$. For PAM-4 signals, the outer ER was measured to be $6.7\,\mathrm{dB}$. The transmitter reference eye diagrams before the burst carver for NRZ and PAM-4 are shown in Fig. 6.

Burst-mode signals with large burst dynamics ($> 20\,\mathrm{dB}$) are generated by carving the continuous signal coming from the MZM into bursts of different lengths and optical powers by means of a semiconductor optical amplifier (SOA), driven by a burst envelope generator. Individual bursts have a duration of $10\,\mu\mathrm{s}$ and a power varying between $-29.3\,\mathrm{dBm}$ and $-4.3\,\mathrm{dBm}$ (for NRZ) and $-26.7\,\mathrm{dBm}$ and $-1.7\,\mathrm{dBm}$ (for PAM-4) and are separated with a $100\,\mathrm{ns}$ guard time. The different arrangement of these bursts follow either a staircase (Fig. 7a), loud-soft (Fig. 7b) or soft-soft (Fig. 7c) pattern, representing typical PON dynamics. The optical signal-to-noise ratio at the SOA output at any burst power level was higher than $30\,\mathrm{dB}$.

A 2-nm-wide optical bandpass filter is used at the transmitter side to suppress out-of-band amplified spontaneous emission (ASE) noise from the SOA carver, and a variable optical attenuator (VOA) is used to adjust the power level of the carved bursts to the target range. The optical signal is then coupled to the lensed APD assembled with the BMTIA. The APD bias is fixed close to the breakdown voltage for optimal responsivity. The electrical waveforms from the BMTIA are AC-coupled and sampled by a $128\,\mathrm{GSa/s}$ real-time-oscilloscope (RTO) with a bandwidth of $40\,\mathrm{GHz}$ for further processing. The RTO acquisitions are triggered by the start of the carving pattern, however no sampling clock synchronization is used between the transmitter and the receiver.

IV. Results and Discussion

A. Frequency Response

The normalized frequency response is obtained by separately estimating the transfer function of the transmitted signal and the BMTIA output signal from the time domain, and then normalizing the output response with the transmitter response. This leaves the net frequency response of the APD and BMTIA. The transmitter frequency response is estimated by observing the SOA output signal with a high-speed reference photodiode (with a bandwidth of $50\,\mathrm{GHz}$) and the RTO. The resulting frequency response is shown in Fig. 8. Using a 25G APD assembly, we achieved a normalized $6\,\mathrm{dB}$ bandwidth of $17.1\,\mathrm{GHz}$ at the sensitivity level and a normalized $6\,\mathrm{dB}$ bandwidth of $24.6\,\mathrm{GHz}$ at the overload level. The difference in bandwidth is due to the constant gain-bandwidth product of the amplifier subcomponents. At sensitivity level, the signal gain of the BMTIA is high, resulting in a lower bandwidth. An additional frequency measurement with a 50G-class APD, assembled on a PCB with our BMTIA IC, shows that the bandwidth limitations are mainly caused by the chosen 25G-class APD.

B. Steady-state BER Performance

To evaluate the BMTIA performance as part of the OLT receiver, steady-state burst-mode BER measurements for 100 Gbit/s PAM-4 and 50 Gbit/s NRZ are performed using the 25G-class APD assembled with our BMTIA. In this section, we look at steady-state conditions as these are not influenced by transients in BMTIA settling, convergence of the clock- and data-recovery (CDR) and equalizer training. In Section IV-C, loud-soft effects are investigated which depend on the guard time between packets. Here, the entire burst is taken into consideration.

A staircase pattern (shown in Fig. 7a) of bursts is generated, and the resulting BMTIA output signals are processed to include a symbol-rate Mueller-Müller CDR and digital equalization using a symbol-spaced 13-tap feedforward equalizer (FFE) and a one-tap decision feedback equalizer (DFE), leading to the eye diagrams shown in Fig. 9. The number of taps are chosen as a trade-off between performance and a realistic complexity for an OLT. To ensure steady-state conditions, a large number of bits (50 kbits, equivalent to $1\,\mu\mathrm{s}$) are discarded to avoid any residual transients. The BER is computed over the remaining equalized payload data in each burst. The resulting BER curves as a function of the OMA are shown in Fig. 10.

For the 50 Gbit/s experiment, the measured sensitivity at a pre-FEC BER threshold of 10^{-2}, expressed in OMA, was $-23.7\,\mathrm{dBm}$ (average power of $-25.9\,\mathrm{dBm}$). The 10^{-2} BER can be lowered to 10^{-12} using a rate-0.84 low-density-parity-check (LDPC) code [3]. The graph also shows 50 Gbit/s unequalized operation, illustrating a $5.5\,\mathrm{dB}$ improvement in sensitivity thanks to the use of digital equalization. The bursts remain under the measured error floor (pre-FEC input BER

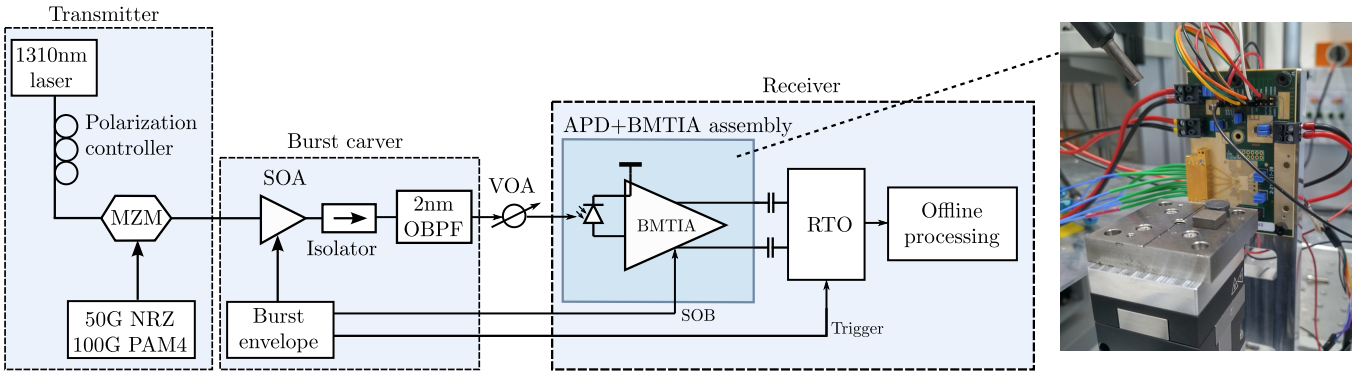

Fig. 5: PON upstream link experimental setup.

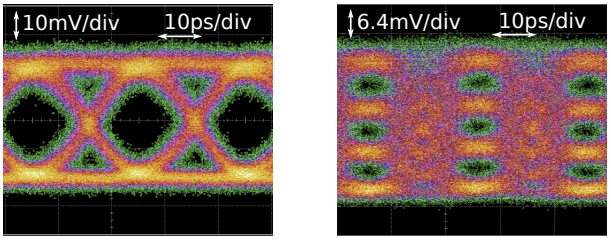

(a) (b)

Fig. 6: 50 Gbit/s NRZ and 100 Gbit/s PAM-4 eye diagrams of optical signal at the transmitter output measured before the burst carver in continuous mode.

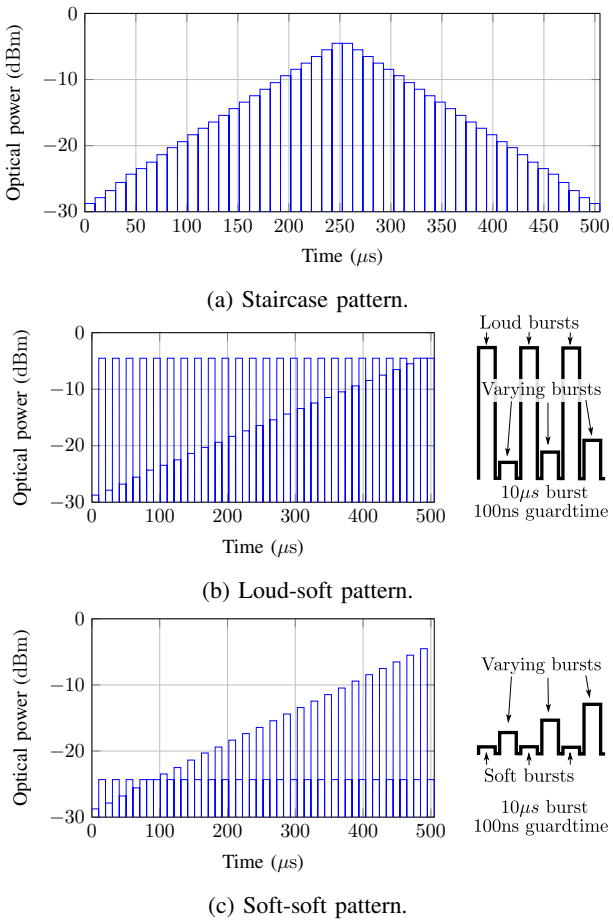

(a) Staircase pattern.

(b) Loud-soft pattern.

(c) Soft-soft pattern.

Fig. 7: Test patterns used for burst carving, represented as the measured optical power at the receiver versus time.

of 10^{-6}) up to at least an OMA of $-4\,\mathrm{dBm}$. As a result, an input dynamic range of at least $21.7\,\mathrm{dB}$ was obtained.
For the 100 Gbit/s PAM-4 experiment, an OMA sensitivity of $-15.8\,\mathrm{dBm}$ (average power of $-17.0\,\mathrm{dBm}$) was obtained at the pre-FEC BER threshold of 10^{-2} and remained below this value up to at least $-0.4\,\mathrm{dBm}$ OMA, resulting in an optical input dynamic range of at least $15.4\,\mathrm{dB}$. The penalty between 100 Gbit/s and 50 Gbit/s was measured to be $7.9\,\mathrm{dB}$ in OMA at a BER of 10^{-2}, similar to values reported in the context of downstream flexible PON using both PAM-4 and NRZ [8].
Fig. 11 shows the resulting output signals as captured by the RTO after a staircase burst pattern. In Fig. 11a, the BMTIA is manually configured in a fixed-gain mode resulting in a varying output signal swing. Fig. 11b shows the same output signal of the BMTIA in its default mode, in which the burst controller activates the automatic gain adaption. The resulting output signals show that the BMTIA settles to a constant voltage swing of $300\,\mathrm{mV}$ peak-to-peak.

C. 50 Gbit/s Loud-Soft Sensitivity Impact

As mentioned in Section II, loud-soft burst transitions are likely to cause sensitivity penalties which depend on the guard time between individual bursts. These penalties are largely caused by the AC-coupling of the BMTIA to the subsequent blocks (in this case the RTO) in combination with imperfect settling of the balancing loop. Charging and discharging of the used AC-coupling capacitors happens at a rate defined by the lower cut-off frequency; if the equilibrium average voltages of two consecutive bursts differ, then an imperfect settling of the balancing loop may cause a sensitivity penalty in the second burst. The reason for this penalty is that the common-mode level of the output of the BMTIA after the AC-coupling is still settling. A fixed bit threshold level will result in a non-optimal choice for the bit decision. Consequentially, it is expected that more bit errors will reside at the beginning of each burst. Therefore in this section, only the first $150\,\mathrm{ns}$ (which is the time needed to finish gain, offset and balancing control in the BMTIA) are discarded, and the remainder of each burst is processed in the same way as before. In addition, the staircase

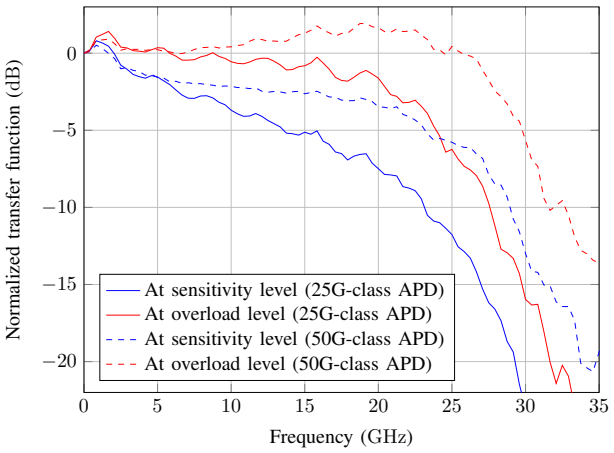

Fig. 8: Bandwidth measurement of the APD-TIA assembly for high and low TIA gain with a 25G-class APD and 50G-class APD.

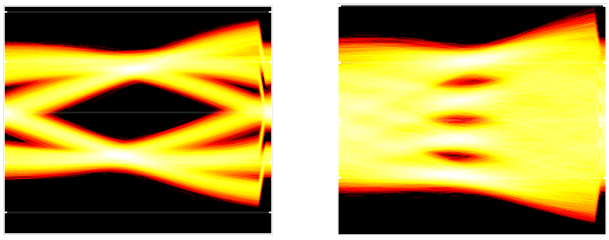

(a) (b)

Fig. 9: 50 Gbit/s NRZ and 100 Gbit/s PAM-4 eye diagrams of the payload part of a burst mode signal at the output of the receiver after digital signal processing (DSP) equalization.

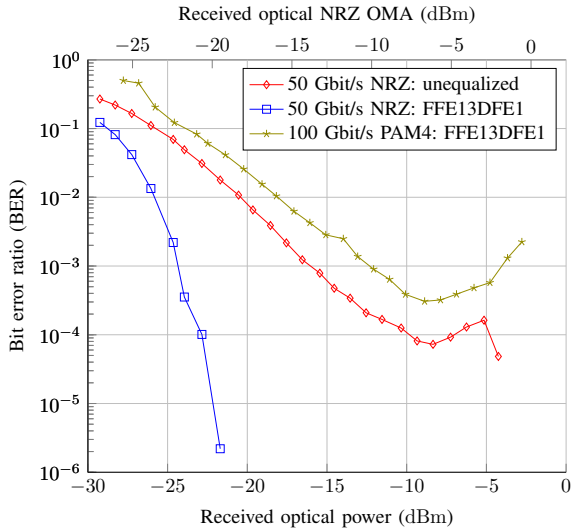

Fig. 10: Steady-state BER as a function of optical power P_{opt} and OMA for 100 Gbit/s PAM-4 and 50 Gbit/s NRZ signals.

patterns used in Fig. 7a are replaced with the patterns shown in Fig. 7b and Fig. 7c to evaluate the impact of loud-soft and soft-soft burst transitions. Finally, the guard time between packets is varied between $100\,\text{ns}$ and $100\,\mu\text{s}$.

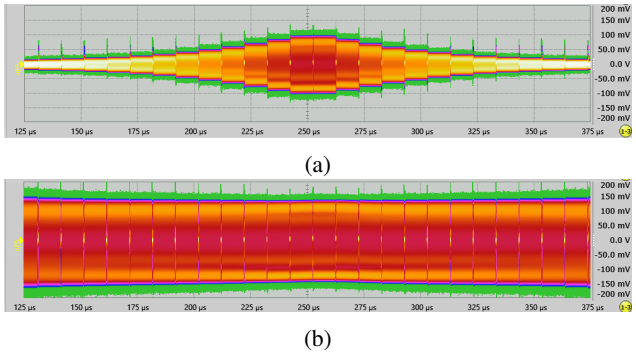

(a) (b)

Fig. 11: Balanced output signals of the BMTIA with a staircase burst pattern, configured in (a) fixed-gain mode and in (b) automatic gain-control mode.

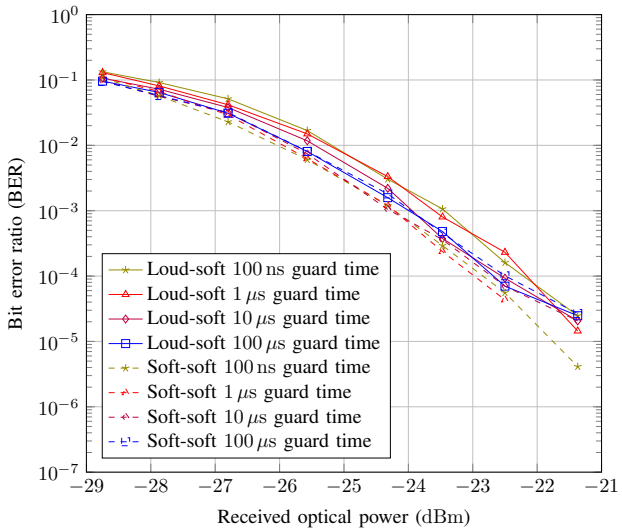

Fig. 12: Bit error ratio as a function of optical power for different guard times for 50 Gbit/s.

Fig. 12 shows the BER performance versus optical burst power for loud-soft ($-4\,\text{dBm}$ average power in the preceding burst) and soft-soft ($-24\,\text{dBm}$ average power in the preceding burst) burst patterns with varying guard times. Fig. 13 shows the resulting optical power penalty versus the used guard time in the loud-soft or soft-soft power pattern for different BER thresholds. For a $100\,\text{ns}$ guard time at a pre-FEC BER threshold of 10^{-2}, a $0.9\,\text{dB}$ loud-soft penalty is obtained. Further decreasing the BER target level to 10^{-3} or 10^{-4} increases the sensitivity power penalty to around $0.7\,\text{dB}$.

D. 50 Gbit/s BER Evolution Within a Packet

Up until now, the aggregate BER of the entire burst is considered. However, as many of the bit errors reside in the beginning of each burst, loud-soft power penalties can simply be reduced by increasing the length of the burst. Therefore, a better way to evaluate loud-soft power penalties is to subdivide the payload of each burst into shorter code words (CWs), which in addition allows us to look how the BER evolves over time.

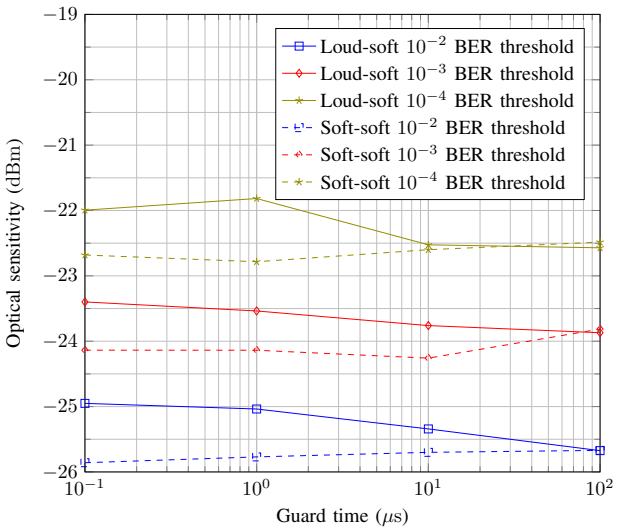

Fig. 13: Optical sensitivity versus guard time for loud-loud and loud-soft patterns with different pre-FEC BER thresholds for 50 Gbit/s.

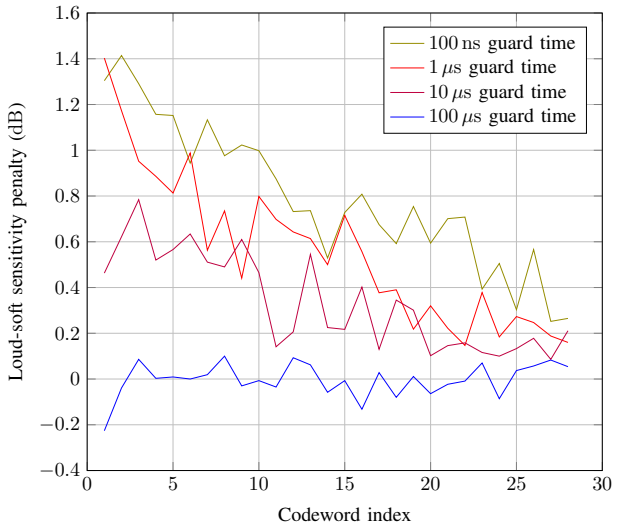

Fig. 14: Evolution of the optical loud-soft sensitivity penalty evaluated per code word over time for loud-soft and soft-soft cases for 50 Gbit/s for varying guard times (100 ns to 100 μs from top to bottom).

Here, code words of 17280 bits (346 ns) are chosen, corresponding to the default LDPC FEC CW size of ITU-T standard G.9804.2 [20]. The training of the equalizer and the bit decision threshold is done on the last 10 CWs and applied to the complete data. This choice of using the last 10 CWs is intended for the equalizer and threshold decision to train on settled data. In practice, this approach could for instance be implemented using historical equalizer coefficients, which are trained on previous bursts, kept in memory and updated on the present burst [21]. The bit errors are counted per CW and for each CW, the penalty in sensitivity of the loud-soft compared to the soft-soft pattern is evaluated.

The resulting loud-soft sensitivity penalty is plotted as a function of the CW index in Fig. 14 for varying guard times. This shows that the worst penalty is at the first CW, as expected. For a 100 ns guard time, the power sensitivity penalty of the first CW is 1.3 dB, compared the aggregate 0.9 dB penalty which is measured over the total burst length. Failure to decode the first CW (which includes the burst header bits) may result in losing the remainder of the burst. Furthermore, it is the worst sensitivity level throughout the burst which is taken into account, and which is setting the requirements for the rest of the system design. For the subsequent CWs, the sensitivity power will gradually converge to the sensitivity power level of the soft-soft pattern with a settling time that approaches the order of the time constants of the high-pass cut-off frequency of the DC-block at the output. Fig. 14 also illustrates that for longer guard times, the penalty in sensitivity is reduced as the AC coupling has enough time to discharge before the start of each burst.

For guard times of 100 μs, the penalty stays around 0 dB. It is noteworthy to point out that, in this experiment, all soft-soft sensitivity curves achieved the same BER-level equal to the measured steady-state sensitivity power of -25.9 dBm shown in Fig. 10.

A simple way to reduce the loud-soft-induced sensitivity penalties is by selectively applying longer guard times when consecutive loud-soft bursts are scheduled. Another solution for reducing the impact of the AC-coupling is to use a self-adapting threshold level for the bit decision, which would track the common-mode level of the samples to optimally recover the transmitted bits. However, this increases the complexity of the DSP.

V. Conclusion

This paper demonstrated a linear BMTIA which, integrated together with a commercial off-the-shelf 25G-class APD, achieved 50 Gbit/s NRZ operation with a sensitivity of -23.7 dBm and dynamic range exceeding 21.7 dB as well as 100 Gbit/s PAM-4 operation with a sensitivity of -15.8 dBm and dynamic range exceeding 15.4 dB, both at a BER of 10^{-2} or lower. Using loud-soft consecutive bursts, with varying guard times, a sensitivity power penalty is observed and illustrated. This penalty is linked to the AC-coupling of the receiver together with imperfect settling of the balancing loop. In the worst case, for a guard time of 100 ns, 1.3 dB of loud-soft penalty is reported. Loud-soft sensitivity penalties eventually converge to the soft-soft burst transition setup. A comparison with other state-of-the-art burst-mode receivers can be found in Section V. We obtained the highest datarate reported to date, while complying with typical PON sensitivity and dynamic range requirements. The achieved results not only demonstrate the viability of a next-generation class of linear BMTIAs needed for 50G PON, but also paves the way for future higher-modulation PON systems requiring linear signal reception in an opportunistically flexible PON context.

Acknowledgment

The authors would like to thank colleagues from Nokia Bell Labs, Murray Hill: Yves Baeyens, Shahriar Shahramian,

TABLE I: Comparison with state-of-the-art.

	[10]	[22]	[17]	[13]	This work
Technology	32nm SOI	28nm	0.25 μm BiCMOS	0.13 μm BiCMOS	0.13 μm BiCMOS
Datarate (/)	25	25	25 / 50	25.78	50 / 100
Power consumption (mW)	109	34.2	280	Not given	285
Sensitivity (dBm)	-12.5	-16	-18.1 / -11.4	-26	-23.7 / -15.8
Dynamic input range (dB)	Not given	5	21.6 / 15.8	23	21.7 / 15.4
Reconfiguration time (ns)	31	2.24	82.7	600	150
Responsivity (A/W)	0.5	4.0	0.5	Not given	9.3

Vincent Houtsma and Dora Van Veen for the discussions, as well as the Modelshop from Nokia Stuttgart for their support.

REFERENCES

[1] R. Bonk, D. Geng, D. Khotimsky, D. Liu, X. Liu, Y. Luo, D. Nesset, V. Oksman, R. Strobel, W. Van Hoof, and J. S. Wey, "50G-PON: The First ITU-T Higher-Speed PON System," *IEEE Communications Magazine*, vol. 60, no. 3, pp. 48–54, 2022.

[2] R. Bonk and T. Pfeiffer, "New Use Cases for PONs Beyond Residential Services," in *2022 Optical Fiber Communications Conference and Exhibition (OFC)*, 2022, pp. 1–3.

[3] ITU-T. (2022) ITU-T Recommendation G.9804.3. [Online]. Available: https://www.itu.int/rec/T-REC-G.9804.3-202109-I/en

[4] X. Yin, G. Coudyzer, P. Ossieur, L. Breyne, B. Van Lombergen, and J. Bauwelinck, "Linear Burst-Mode Receivers for DSP-Enabled Passive Optical Networks," in *2021 Optical Fiber Communications Conference and Exhibition (OFC)*, 2021, pp. 1–3.

[5] G. Coudyzer, P. Ossieur, L. Breyne, A. La Porta, S. Paredes, J. Bauwelinck, and X. Yin, "Study of Burst-Mode Adaptive Equalization for >25G PON Applications [Invited]," *IEEE/OSA Journal of Optical Communications and Networking*, vol. 12, no. 1, pp. A104–A112, January 2020.

[6] R. Borkowski, H. Schmuck, G. Cerulo, J.-G. Provost, V. Houtsma, D. van Veen, E. Harstead, F. Mallecot, and R. Bonk, "The Impact of Transmitter Chirp Parameter on the Power Penalty and Design of 50 Gbit/s TDM-PON," in *2020 Optical Fiber Communications Conference and Exhibition (OFC)*, 2020, pp. 1–3.

[7] J. Potet, M. Gay, L. Bramerie, H. Hallak Elwan, F. Saliou, G. Simon, and P. Chanclou, "Real Time 100 Gbit/s/λ PAM-4 Experiments for Future Access Networks over 20 km with 29 dB Optical Budget," in *2021 European Conference on Optical Communication (ECOC)*, 2021, pp. 1–3.

[8] R. Borkowski, Y. Lefevre, A. Mahadevan, D. van Veen, M. Straub, R. Kaptur, B. Czerwinski, B. Cornaglia, V. Houtsma, W. Coomans, R. Bonk, and J. Maes, "FLCS-PON—an opportunistic 100 Gbit/s flexible PON prototype with probabilistic shaping and soft-input FEC: operator trial and ODN case studies," *Journal of Optical Communications and Networking*, vol. 14, no. 6, pp. C82–C91, 2022.

[9] G. Simon, F. Saliou, J. Potet, P. Chanclou, R. Rosales, I. N. Cano, and D. Nesset, "50Gb/s Real-Time Transmissions with Upstream Burst-Mode for 50G-PON using a Common SOA Pre-amplifier/Booster at the OLT," in *2022 Optical Fiber Communications Conference and Exhibition (OFC)*, 2022, pp. 1–3.

[10] A. Rylyakov, J. Proesel, S. Rylov, B. Lee, J. Bulzacchelli, A. Ardey, B. Parker, M. Beakes, C. Baks, C. Schow, and M. Meghelli, "A 25Gb/s burst-mode receiver for rapidly reconfigurable optical networks," in *2015 IEEE International Solid-State Circuits Conference - (ISSCC) Digest of Technical Papers*, 2015, pp. 1–3.

[11] I. Ozkaya, A. Cevrero, P. A. Francese, C. Menolfi, M. Braendli, T. Morf, D. Kuchta, L. Kull, M. Kossel, D. Luu, M. Meghelli, Y. Leblebici, and T. Toifl, "A 56Gb/s burst-mode NRZ optical receiver with 6.8ns power-on and CDR-Lock time for adaptive optical links in 14nm FinFET CMOS," in *2018 IEEE International Solid - State Circuits Conference - (ISSCC)*, 2018, pp. 266–268.

[12] H. Zheng, A. Shen, N. Cheng, N. Chand, F. Effenberger, and X. Liu, "High-Performance 50G-PON Burst-Mode Upstream Transmission at 25 Gb/s with DSP-Assisted Fast Burst Synchronization and Recovery," in *2019 Asia Communications and Photonics Conference (ACP)*, 2019, pp. 1–3.

[13] N. Tanaka, D. Umeda, Y. Sugimoto, T. Funada, K. Tanaka, and S. Ogita, "25.78-Gbit/s Burst-mode Receiver for 50G-EPON OLT," in *2020 Optical Fiber Communications Conference and Exhibition (OFC)*, 2020, pp. 1–3.

[14] H. Katsurai, Y. Nakanishi, A. Kanda, T. Yoshimatsu, S. Kanazawa, M. Nada, H. Nakamura, and K. Sano, "A 25G Burst-mode Receiver with -27.7-dBm Sensitivity and 150-ns Response-Time for 50G-EPON Systems," in *2020 European Conference on Optical Communications (ECOC)*, 2020, pp. 1–3.

[15] P. Ossieur, N. A. Quadir, S. Porto, C. Antony, W. Han, M. Rensing, P. O'Brien, and P. D. Townsend, "A 10 Gb/s Linear Burst-Mode Receiver in 0.25 μm SiGe:C BiCMOS," *IEEE Journal of Solid-State Circuits*, vol. 48, no. 2, pp. 381–390, 2013.

[16] M. D. Santa, C. Antony, M. Power, A. Jain, P. Ossieur, G. Talli, and P. D. Townsend, "25Gb/s PAM4 burst-mode system for upstream transmission in passive optical networks," in *2017 Optical Fiber Communications Conference and Exhibition (OFC)*, 2017, pp. 1–3.

[17] G. Coudyzer, P. Ossieur, J. Bauwelinck, and X. Yin, "A 25Gbaud PAM-4 Linear Burst-Mode Receiver With Analog Gain- and Offset Control in 0.25um SiGe:C BiCMOS," *IEEE Journal of Solid-State Circuits*, vol. 55, no. 8, pp. 2206–2218, 2020.

[18] G. Coudyzer, P. Ossieur, L. Breyne, M. Matters, J. Bauwelinck, and X. Yin, "A 50 Gbit/s PAM-4 Linear Burst-Mode Transimpedance Amplifier," *IEEE Photonics Technology Letters*, vol. 31, no. 12, pp. 951–954, 2019.

[19] T. Gurne, G. Coudyzer, B. Van Lombergen, R. Borkowski, M. Verplaetse, M. Straub, Y. Lefevre, P. Ossieur, R. Bonk, W. Coomans, X. Yin, and J. Maes, "First Demonstration of a 100 Gbit/s PAM-4 Linear Burst-Mode Transimpedance Amplifier for Upstream Flexible PON," in *2022 European Conference on Optical Communication (ECOC)*, 2022.

[20] ITU-T. (2022) ITU-T Recommendation G.9804.2. [Online]. Available: https://www.itu.int/rec/T-REC-G.9804.2-202109-P

[21] T. Kanai, M. Fujiwara, R. Igarashi, N. Iiyama, R. Koma, J. ichi Kani, and T. Yoshida, "Symmetric 10 Gbit/s 40-km reach DSP-based TDM-PON with a power budget over 50dB," *Opt. Express*, vol. 29, no. 11, pp. 17 499–17 509, May 2021. [Online]. Available: https://opg.optica.org/oe/abstract.cfm?URI=oe-29-11-17499

[22] K. C. Chen and A. Emami, "A 25-Gb/s Avalanche Photodetector-Based Burst-Mode Optical Receiver With 2.24-ns Reconfiguration Time in 28-nm CMOS," *IEEE Journal of Solid-State Circuits*, vol. 54, no. 6, pp. 1682–1693, 2019.